The guanylate kinase domain of the β-subunit of voltage-gated calcium channels suffices to modulate gating

Giovanni Gonzalez-Gutierrez*, Erick Miranda-Laferte*, Doreen Nothmann*, Silke Schmidt*, Alan Neely[†‡], and Patricia Hidalgo*[‡]

*Institut für Neurophysiologie, Medizinische Hochschule Hannover, 30625 Hannover, Germany; and [†]Centro de Neurociencia de Valparaíso, Universidad de Valparaíso, Valparaíso 2349400, Chile

Communicated by Ramón Latorre, Centro de Estudios Científicos, Valdivia, Chile, July 9, 2008 (received for review March 19, 2008)

Inactivation of voltage-gated calcium channels is crucial for the spatiotemporal coordination of calcium signals and prevention of toxic calcium buildup. Only one member of the highly conserved family of calcium channel β-subunits—$Ca_V\beta$—inhibits inactivation. This unique property has been attributed to short variable regions of the protein; however, here we report that this inhibition actually is conferred by a conserved guanylate kinase (GK) domain and, moreover, that this domain alone recapitulates $Ca_V\beta$-mediated modulation of channel activation. We expressed and refolded the GK domain of $Ca_V\beta_{2a}$, the unique variant that inhibits inactivation, and of $Ca_V\beta_{1b}$, an isoform that facilitates it. The refolded domains of both $Ca_V\beta$ variants were found to inhibit inactivation of $Ca_V2.3$ channels expressed in *Xenopus laevis* oocytes. These findings suggest that the GK domain endows calcium channels with a brake restraining voltage-dependent inactivation, and thus facilitation of inactivation by full-length $Ca_V\beta$ requires additional structural determinants to antagonize the GK effect. We found that $Ca_V\beta$ can switch the inactivation phenotype conferred to $Ca_V2.3$ from slow to fast after posttranslational modifications during channel biogenesis. Our findings provide a framework within which to understand the modulation of inactivation and a new functional map of $Ca_V\beta$ in which the GK domain regulates channel gating and the other conserved domain (Src homology 3) may couple calcium channels to other signaling pathways.

auxiliary subunit | modular structure | regulation

Calcium signals mediate various cellular processes, including neurotransmission, excitation-contraction coupling, hormone secretion, and gene expression (1). Voltage-gated calcium channels (VGCCs) are activated and inactivated on membrane depolarization, allowing transient increases in cytosolic Ca^{2+} concentration. Voltage-dependent activation and inactivation of VGCCs depend strongly on the association of the ancillary β-subunit ($Ca_V\beta$) to a highly conserved sequence within the intracellular loop joining the first and second repeats (loop I-II) of the pore-forming subunit ($Ca_V\alpha_1$), known as the α-interaction domain (AID) (2). $Ca_V\beta$ is encoded by four nonallelic genes (β_{1-4}), each with multiple splice variants. Except for a few short splicing forms (3), all of these genes share a common structural arrangement, consisting of two highly conserved regions separated and flanked by shorter variable sequences (Fig. 1*A*). Crystallographic studies have revealed that whereas the first region encompasses a Src homology 3 (SH3) domain, the second region encompasses a guanylate kinase (GK) domain. The AID sequence forms an α-helix that fits into a hydrophobic cleft of the GK module that lies on the opposite side of the SH3 domain (Fig. 1*B*) (4–6). This suggests that the isolated GK module may preserve at least some of the modulatory capabilities of the full $Ca_V\beta$.

Despite several attempts to use different $Ca_V\beta$ constructs and experimental approaches (7–11), the functional competence of isolated GK and its ability to mimic $Ca_V\beta$ function remain incompletely understood. A contributing factor may be the reduced stability of some GK-containing constructs (11). To overcome this difficulty, we expressed and refolded the GK domain of two $Ca_V\beta$ isoforms, $Ca_V\beta_{1b}$ and $Ca_V\beta_{2a}$. These isoforms share modulatory effects on voltage-dependent activation and exhibit opposite actions on voltage-dependent inactivation. We studied the effect of the refolded GK modules on *Xenopus* oocytes expressing two types of α_1 pore-forming subunits ($Ca_V1.2$ and $Ca_V2.3$) and compared it with the action of the recombinant full length and also the core of the $Ca_V\beta$ protein containing both SH3 and GK domains. Whereas $Ca_V\beta_{2a}$ is unique in its ability to inhibit voltage-dependent inactivation, the other $Ca_V\beta$ isoforms facilitate this inactivation (12–17). $Ca_V\beta_{2a}$ decelerates inactivation, increases the fraction of noninactivating current, and shifts the steady-state inactivation curve toward more positive potentials. These distinguishing modulatory properties of $Ca_V\beta_{2a}$ have been broadly attributed to palmitoylation of the two contiguous cysteine residues at positions 3 and 4 in the N terminus region (15, 18–20). Here, however, we report that instead, the GK modules derived from both $Ca_V\beta_{2a}$ and $Ca_V\beta_{1b}$ inhibit inactivation of $Ca_V2.3$ channels. This finding indicates that the structural determinants of inhibition of inactivation by $Ca_V\beta_{2a}$ are encoded not in variable regions but rather within the GK domain. GK appears to endow calcium channels with a brake to impair voltage-dependent inactivation; therefore, masking the inhibitory effect of GK facilitates inactivation. We show that $Ca_V\beta$ acquires this capability when co-expressed with $Ca_V\alpha_1$ but not when added later during channel biogenesis. Moreover, $Ca_V\beta_{2a}$-GK increases peak currents and shifts the activation curve toward more negative potentials of $Ca_V1.2$ channels. Thus, GK emerges as a functional unit that recapitulates the hallmarks of $Ca_V\beta$ modulation.

Results

Refolding and Binding Assay of $Ca_V\beta$-GK Domain. The GK domain derived from $Ca_V\beta_{1b}$ ($Ca_V\beta_{1b}$-GK) and $Ca_V\beta_{2a}$ ($Ca_V\beta_{2a}$-GK) (Fig. 1*A*) were expressed in bacteria, where they accumulated in inclusion bodies and were refolded by batch dilution. The purified GK domains were concentrated up to 0.1 mg/ml, because further concentration resulted in progressive protein aggregation, as demonstrated by high–molecular mass peaks

Author contributions: G.G.-G., E.M.-L., A.N., and P.H. designed research; G.G.-G., E.M.-L., D.N., and S.S. performed research; G.G.-G., E.M.-L., A.N., and P.H. analyzed data; and A.N. and P.H. wrote the paper.

The authors declare no conflict of interest.

This article is a PNAS Direct Submission.

[‡]To whom correspondence may be addressed. E-mail: alan@cnv.cl or hidalgo.patricia@mh-hannover.de.

This article contains supporting information online at www.pnas.org/cgi/content/full/0806558105/DCSupplemental.

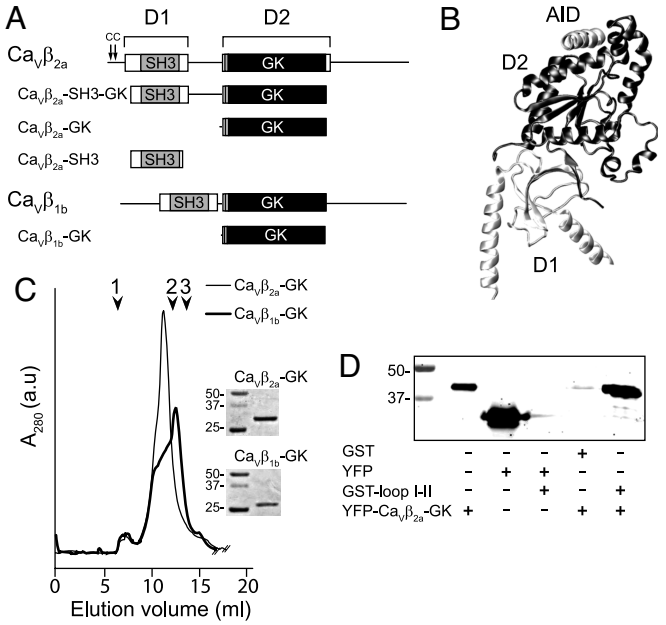

Fig. 1. Domain structure, purification, and binding assay of $Ca_V\beta$ constructs. (*A*) Schematic representation of $Ca_V\beta_{2a}$, $Ca_V\beta_{1b}$, and derived protein constructs used in this study. $Ca_V\beta$ consists of two highly conserved regions, D1 and D2 (boxes), which are connected and flanked by variable regions (continuous lines). The gray box is the SH3 module; the black box is the GK module. The two cysteine residues at the N terminus of $Ca_V\beta_{2a}$ that undergo palmitoylation are indicated by arrows. (*B*) A ribbon diagram of the crystal structure of $Ca_V\beta$ in complex with AID (PDB accession code 1T3L). (*C*) Size-exclusion chromatography elution profile on the Superdex 200 10/30 column (GE Healthcare) of refolded $Ca_V\beta_{2a}$-GK and $Ca_V\beta_{1b}$-GK. Here 1 indicates the void volume, 2 indicates the elution volume of albumin (67 kDa), and 3 indicates the elution volume of ovalbumin (43 kDa). The inset shows Coomassie-stained sodium dodecyl sulfate polyacrylamide gel electrophoresis (SDS/PAGE) gels of the indicated proteins. Numbers indicate the molecular mass of standards, in kDa. (*D*) SDS/PAGE gel of the binding reaction with the indicated proteins. Yellow fluorescence protein (YFP)-$Ca_V\beta_{2a}$-GK is seen to bind specifically to GST–loop I-II (last lane). The binding assay was repeated three times.

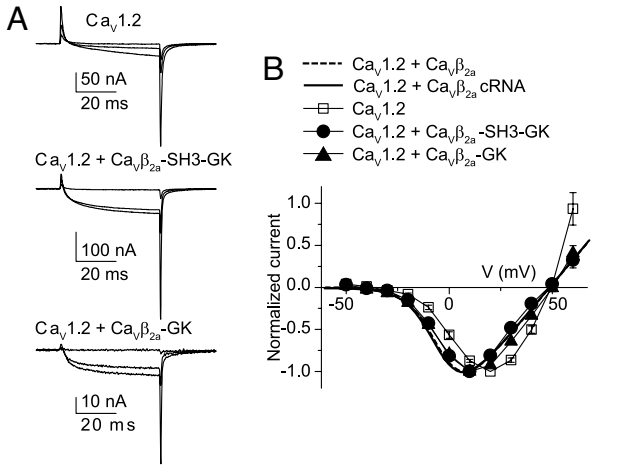

Fig. 2. Refolded $Ca_V\beta_{2a}$-GK and $Ca_V\beta_{2a}$-SH3-GK shift the current–voltage relationship of $Ca_V1.2$-mediated currents. (*A*) Representative gating and ionic currents traces from oocytes expressing $Ca_V1.2$ cRNA alone and after injection of either $Ca_V\beta_{2a}$-SH3-GK or $Ca_V\beta_{2a}$-GK. Currents were evoked by 50-ms pulses to −30, 0, and +30 mV from a holding potential of −80 mV. (*B*) Normalized current–voltage plot from oocytes expressing the subunit combinations $Ca_V1.2$ cRNA (n = 11), $Ca_V1.2$ + $Ca_V\beta_{2a}$-SH3-GK (n = 14), and $Ca_V1.2$ + $Ca_V\beta_{2a}$-GK (n = 16). For comparison, normalized current–voltage curves for $Ca_V1.2$ + $Ca_V\beta_{2a}$, either injected as a protein (dashed line) or co-injected as cRNA (continuous line) are shown (see Table S1 for details).

appearing in the void volume of the size-exclusion chromatography column. At 0.1 mg/ml, $Ca_V\beta_{2a}$-GK eluted from the size-exclusion chromatography in a predominant peak, whereas $Ca_V\beta_{1b}$-GK exhibited a shoulder at this position and a main peak eluting near the albumin peak (Fig. 1*C*). Both GK constructs migrated with an apparent molecular mass larger than that predicted by their amino acid sequences. This may reflect either an aberrant migration or formation of higher oligomeric states. To determine whether the refolded GK domains form multimers, we conducted a sucrose gradient analysis [supporting information (SI) Figs. S1–S3]. The $Ca_V\beta_{2a}$-GK distribution overlapped with a protein standard of 66 kDa, whereas $Ca_V\beta_{1b}$-GK appeared over a wider range, reaching a second standard of 29 kDa. Thus, our data are consistent with $Ca_V\beta_{2a}$-GK being essentially a dimer and $Ca_V\beta_{1b}$-GK being a mixture of dimers and monomers.

To assess the binding ability of $Ca_V\beta_{2a}$-GK to loop I-II, we fused the former to YFP (YFP-$Ca_V\beta_{2a}$-GK) and the latter to GST (GST–loop I-II). $Ca_V\beta_{2a}$-GK was seen to bind specifically to loop I-II; no association between GST and YFP-$Ca_V\beta_{2a}$-GK or between YFP and GST–loop I-II was detected (Fig. 1*D*).

$Ca_V\beta_{2a}$-GK Increases Peak Current Amplitude and Shifts the Current–Voltage Relationship of $Ca_V1.2$ Channels. To investigate the modulation of voltage-dependent activation by $Ca_V\beta_{2a}$-GK, we used the $Ca_V1.2\alpha_1$ subunit, because it exhibits little inactivation, and the coupling between voltage sensor and channel opening is extremely sensitive to the presence of $Ca_V\beta$. This $Ca_V\alpha_1$ isoform also is more suitable for monitoring channel expression through gating current measurements (21). Injection of recombinant full-length $Ca_V\beta_{2a}$ into oocytes expressing $Ca_V1.2$ channels results in an increase in the ionic current to charge movement ratio (I/Q) and a leftward shift in the current–voltage relationship (22). $Ca_V\beta_{2a}$-SH3-GK proved to be equally robust in modulating the activation of $Ca_V1.2$ channels (Fig. 2*A*, Fig. S4, and Table S1). Here, as in a previous report (22), we measured charge movement by integrating outward transient currents at the onset of depolarizing pulses to the ionic current reversal potential. Injection of $Ca_V\beta_{2a}$-SH3-GK into $Ca_V1.2$-expressing oocytes increased the I/Q from 0.3 ± 0.06 nA/pC (n = 15) to 4.6 ± 0.7 nA/pC (n = 17), comparable to the values obtained after injection of $Ca_V\beta_{2a}$ (4.5 ± 0.9 nA/pC; n = 18). The effect of $Ca_V\beta_{2a}$-GK was seen more clearly at reduced channel expression levels, where gating currents were barely visible and thus I/Q plots were not readily measurable. Nevertheless, the normalized current–voltage relationship was shifted to more-negative potentials and to similar extents with $Ca_V\beta_{2a}$ (as protein or cRNA), $Ca_V\beta_{2a}$-SH3-GK, and $Ca_V\beta_{2a}$-GK (Fig. 2*B*).

We attribute the limited activity of refolded $Ca_V\beta_{2a}$-GK to the low concentration of this protein, calculated as 0.3 μM for a 525-nl oocyte. In addition, at high expression levels, a large amount of $Ca_V1.2$ subunit remained in the cytoplasm and may have acted as a sink. Another contributing factor could be the protein's decreased stability (see below). To overcome this potential problem, and inspired by a previous experiment demonstrating that $Ca_V\beta_{2a}$ recapitulates channel modulation when attached to the C-termini of $Ca_V\alpha_1$ (23), we covalently linked $Ca_V\beta$-GK to $Ca_V1.2$ ($Ca_V1.2$-$Ca_V\beta_{2a}$-GK) and compared this with $Ca_V1.2$ linked to $Ca_V\beta_{2a}$ ($Ca_V1.2$-$Ca_V\beta_{2a}$). Fig. 3 shows gating and ionic currents from oocytes expressing $Ca_V1.2$-$Ca_V\beta_{2a}$ or $Ca_V1.2$-$Ca_V\beta_{2a}$-GK. When covalently linked to $Ca_V1.2$, $Ca_V\beta_{2a}$-GK appears to be as efficient as full-length $Ca_V\beta_{2a}$ in increasing I/Q and shifting the voltage dependence of activation. This effect was abolished by a mutation in the

PHYSIOLOGY

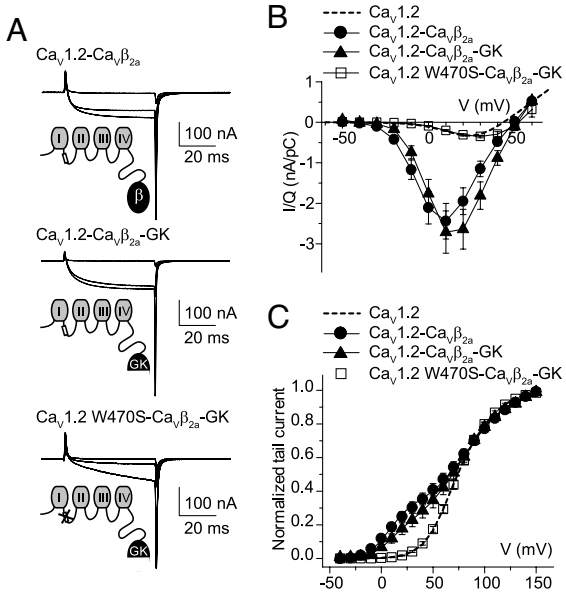

Fig. 3. Ca$_V\beta_{2a}$-GK covalently linked to Ca$_V$1.2 WT, but not to Ca$_V$1.2 W470S, increases peak current amplitudes and shifts the current–voltage relationship. (*A*) Representative gating and ionic current traces from oocytes expressing Ca$_V$1.2 WT covalently linked to either Ca$_V\beta_{2a}$ (Ca$_V$1.2-Ca$_V\beta_{2a}$) or Ca$_V\beta_{2a}$-GK (Ca$_V$1.2-Ca$_V\beta_{2a}$-GK), and Ca$_V$1.2 W470S covalently linked to Ca$_V\beta_{2a}$-GK (Ca$_V$1.2 W470S-Ca$_V\beta_{2a}$-GK). Currents were evoked by 50-ms pulses to −30, 0, and +30 mV from a holding potential of −80 mV. (*B*) Ionic current from oocytes expressing the different constructs were normalized by charge movement (I/Q) and plotted versus voltage. For Ca$_V$1.2-Ca$_V\beta_{2a}$, the peak I/Q was 2.44 ± 0.44 nA/pC (n = 17); for Ca$_V$1.2-Ca$_V\beta_{2a}$-GK, it was 2.71 ± 0.52 nA/pC (n = 17); and for Ca$_V$1.2 W470S-Ca$_V\beta_{2a}$-GK, it was 0.35 ± 0.03 nA/pC (n = 17). For comparison, the average I/Q from 15 oocytes expressing Ca$_V$1.2 alone are shown as dashed lines (0.30 ± 0.06 nA/pC). (*C*) Normalized tail currents from oocytes expressing the different constructs. The continuous lines correspond to the fit of the sum of two Boltzmann distributions, and the dashed line corresponds to the fit obtained from Ca$_V$1.2-expressing oocytes (see Fig. S4 and Table S1 for details). The fit to Ca$_V$1.2 W470S-Ca$_V\beta_{2a}$-GK was excluded from the plot for clarity.

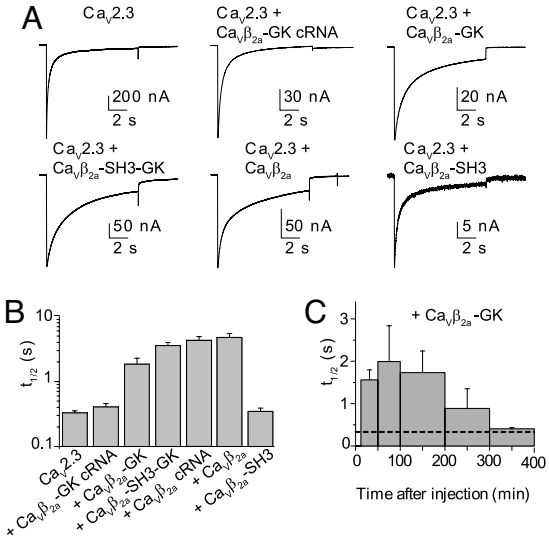

Fig. 4. Ca$_V\beta$-GK slows inactivation of Ca$_V$2.3-mediated currents. (*A*) Representative current traces from oocytes expressing Ca$_V$2.3 cRNA alone or after injection of the specified protein during a 10-s pulse to 0 mV from a holding potential of −90 mV. (*B*) Average decay times to half-peak current amplitude (t½) for the different subunit combinations: Ca$_V$2.3 cRNA, t½ = 0.33 ± 0.03 s (n = 26); Ca$_V$2.3 + Ca$_V\beta_{2a}$-GK cRNA, t½ = 0.41 ± 0.05 s (n = 13); Ca$_V$2.3 + Ca$_V\beta_{2a}$-GK, t½ = 1.85 ± 0.44 s (n = 13); Ca$_V$2.3 + Ca$_V\beta_{2a}$-SH3-GK, t½ = 3.57 ± 0.42 s (n = 21); Ca$_V$2.3 + Ca$_V\beta_{2a}$ cRNA, t½ = 4.11 ± 0.65 s (n = 12); Ca$_V$2.3 + Ca$_V\beta_{2a}$, t½ = 4.76 ± 0.70 s (n = 16); Ca$_V$2.3 + Ca$_V\beta_{2a}$-SH3, t½ = 0.35 ± 0.04 s (n = 13). The t½ values for Ca$_V$2.3 + Ca$_V\beta_{2a}$-GK, Ca$_V$2.3 + Ca$_V\beta_{2a}$-SH3-GK, and Ca$_V$2.3 + Ca$_V\beta_{2a}$ were significantly different from those measured in oocytes expressing Ca$_V$2.3 alone (t test; $P < .01$). (*C*) Time course of inhibition of inactivation by Ca$_V\beta_{2a}$-GK. Each bar corresponds to the average t½ measured at different time intervals after protein injection. The first bar includes recordings from 12–50 min (n = 4), and the second bar includes recordings from 51–100 min (n = 6) and every 100 min thereafter (n = 7, 2, and 4, respectively). The dashed line corresponds to t½ for Ca$_V$2.3 alone.

conserved tryptophan within the AID (W470S) shown to prevent binding to Ca$_V\beta$ (22), indicating that the changes in gating properties occurred through specific association of the fused GK moiety to the AID site and not from changes in channel activity generated by the GK linkage.

Ca$_V\beta_{2a}$-GK Inhibits Inactivation of Ca$_V$2.3 WT Channels. Next, we investigated the ability of Ca$_V\beta_{2a}$-GK to regulate inactivation kinetics, using the fast-inactivating Ca$_V$2.3 channels (Fig. 4). Injection of refolded Ca$_V\beta_{2a}$-GK into Ca$_V$2.3-expressing oocytes resulted in a sixfold increase in the decay time to half-peak current amplitude (t½; Fig. 4 *A* and *B*); however, Ca$_V\beta_{2a}$-GK co-injected as cRNA failed to modulate the Ca$_V$2.3-mediated currents. A greater increase in t½ was observed after injection of full-length Ca$_V\beta_{2a}$, either as protein or co-injected as cRNA, and Ca$_V\beta_{2a}$-SH3-GK. Consistent with our earlier findings, Ca$_V\beta_{2a}$-SH3 decreased ionic currents without changing the time course (24). The effect of refolded Ca$_V\beta_{2a}$-GK vanished 5 h after injection, indicating some degree of protein instability (Fig. 4*C*); this finding also may explain the lack of effect of Ca$_V\beta_{2a}$-GK cRNA.

Both Ca$_V\beta_{2a}$-GK and Ca$_V\beta_{2a}$-SH3-GK shifted the steady-state inactivation curve of Ca$_V$2.3-mediated currents to more positive potentials. A residual current at the end of the pulse also emerged, but it was only a fraction of that seen with full-length Ca$_V\beta_{2a}$ (Fig. 5). Half-inactivation voltages (V½), derived from the fit to a Boltzmann distribution plus the residual component, were similar with Ca$_V\beta_{2a}$-GK, Ca$_V\beta_{2a}$-SH3-GK, and full-length Ca$_V\beta_{2a}$ but were significantly more positive than those with Ca$_V$2.3 alone (Fig. 5*B* and Table S2). Overall, Ca$_V\beta_{2a}$ derivatives appear to be less effective than full-length Ca$_V\beta_{2a}$ in inhibiting inactivation and may reflect a contribution of unoccupied Ca$_V$2.3 subunits. Nevertheless, inactivation of Ca$_V$2.3 channels bearing the W386S mutation that disrupt binding to Ca$_V\beta$ (25) were not modulated by Ca$_V\beta_{2a}$ or Ca$_V\beta_{2a}$-GK (Fig. S5), indicating that the action of Ca$_V\beta_{2a}$-GK is AID-dependent and does not involve nonspecific binding. As in previous work (25), we also found that this substitution results in Ca$_V$2.3 channels that inactivate more slowly than wild-type channels. Taken together, these findings indicate that the N terminus of Ca$_V\beta_{2a}$ is not mandatory for inhibiting inactivation and predict (owing to the highly conserved nature of the GK domain) that inhibition of inactivation is a property shared by all GKs in the various Ca$_V\beta$ isoforms.

Ca$_V\beta_{1b}$-GK Resembles Ca$_V\beta_{2a}$ in Inhibiting Inactivation of Ca$_V$2.3 WT Channels. We studied the effect of a GK module derived from Ca$_V\beta_{1b}$, an isoform that accelerates inactivation and shifts the steady-state inactivation curve to more negative potentials when co-expressed as cRNA (12). Injection of refolded Ca$_V\beta_{1b}$-GK into oocytes expressing Ca$_V$2.3 channels yielded currents that inactivated slowly (t½ = 4.2 ± 0.9 s, n = 16; Fig. 6*A*). Ca$_V\beta_{1b}$-GK also shifted the steady-state inactivation curves toward more depolarizing potentials and, like Ca$_V\beta_{2a}$-GK, induced a residual current (Fig. 6 *B* and *C*). Based on these findings, we conclude that the GK module encompasses the minimal structural re-

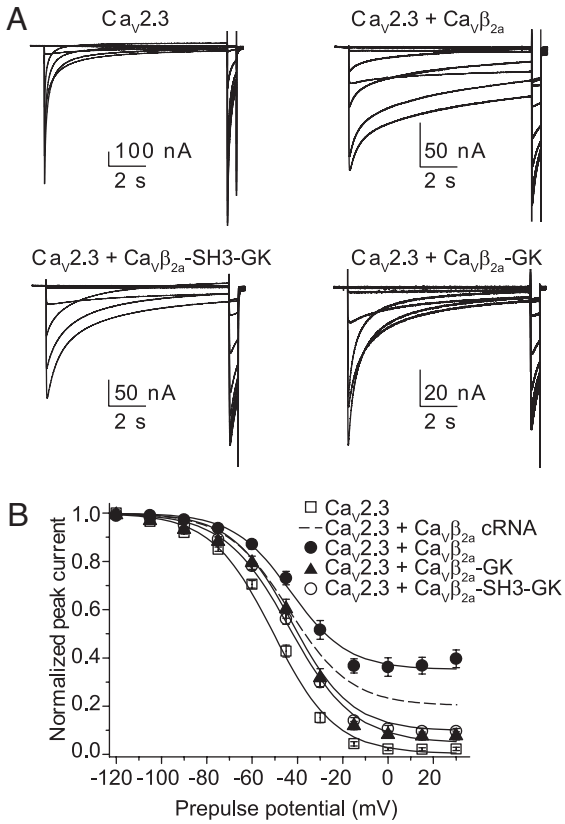

Fig. 5. Ca$_V\beta$-GK shifts midpoint voltage for the steady-state inactivation of Ca$_V$2.3-mediated currents. (*A*) Representative traces of Ca$_V$2.3-mediated currents in the presence of the specified protein during a steady-state inactivation pulse protocol. This consisted of a 10-s conditioning period to voltages of increasing amplitude, from −120 mV to +30 mV in 15-mV increments, followed by a 0.4-s test pulse to 0 mV. Pulses were delivered once every 50 s from a holding potential of −90 mV. (*B*) Average steady-state inactivation curves from oocytes expressing Ca$_V$2.3 alone ($n = 22$) or after injection of full-length Ca$_V\beta_{2a}$ ($n = 13$), Ca$_V\beta_{2a}$-SH3-GK ($n = 23$), or Ca$_V\beta_{2a}$-GK ($n = 15$). The continuous lines correspond to Boltzmann distributions plus a noninactivating current component that best described each set of data. For comparison, the Boltzmann distributions that best described the Ca$_V$2.3 + Ca$_V\beta_{2a}$ cRNA data (dashed line) also are shown. The V½ values for Ca$_V$2.3 + Ca$_V\beta_{2a}$-GK and Ca$_V$2.3 + Ca$_V\beta_{2a}$-SH3-GK are significantly different than the V½ measured in oocytes expressing Ca$_V$2.3 alone (*t* test; $P < .01$) (see Table S2 for details).

quirements to inhibit voltage-dependent inactivation. A question that naturally arises is what determines the facilitation of inactivation by full-length Ca$_V\beta$ proteins.

Full-Length Ca$_V\beta$ Proteins Switch Ca$_V$2.3-Inactivation Phenotype Depending on the Time of Injection. Our finding that the GK module inhibits inactivation implies that full-length proteins that facilitate inactivation must be able to counteract the GK effect. This property has been documented for Ca$_V$2.3 channels coexpressed with cRNA encoding full-length Ca$_V\beta_{1b}$ or a palmitoylation-deficient mutant of Ca$_V\beta_{2a}$ bearing two cysteine-to-serine substitutions at positions 3 and 4 (Ca$_V\beta_{2a}$ C3,4S) (12, 18). Here we report that injection of these Ca$_V\beta$ constructs as proteins into oocytes already expressing Ca$_V$2.3 channels (late injection) slowed the time to inactivation compared with Ca$_V$2.3 alone (Fig. 7 *A* and *B*). Furthermore, Ca$_V\beta$ C3,4S shifted the steady-state inactivation curve toward more positive potentials (Fig. 7 *C* and *D* and Table S2). Assuming that these full-length proteins were folded correctly, we conjectured that posttranslational modifications requiring longer times than allowed by the experiment were needed to confer their native phenotype.

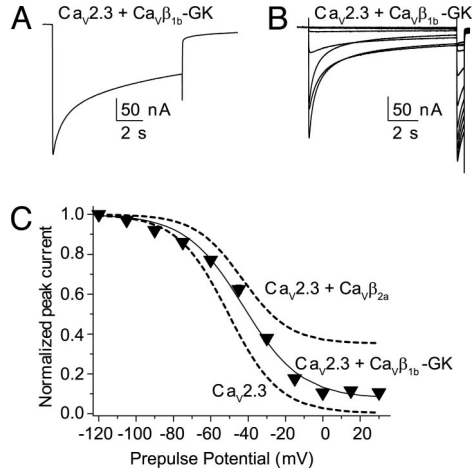

Fig. 6. Ca$_V\beta_{1b}$-GK slows inactivation of Ca$_V$2.3-mediated currents and shifts the steady-state inactivation toward more depolarized potentials. (*A*) Representative current traces from a Ca$_V$2.3-expressing oocytes injected with Ca$_V\beta_{1b}$-GK during a 10-s pulse to 0 mV from a holding potential of −90 mV. (*B*) Current traces evoked with the steady-state inactivation pulse protocol from the same oocytes shown in (*A*). (*C*) Average steady-state inactivation curve from oocytes expressing Ca$_V$2.3 and injected with Ca$_V\beta_{1b}$-GK protein ($n = 14$). For comparison, the Boltzmann distributions that best describe Ca$_V$2.3 and Ca$_V$2.3 + Ca$_V\beta_{2a}$ data from Fig. 5 also are shown (dashed lines). The V½ value for Ca$_V$2.3 + Ca$_V\beta_{1b}$-GK was significantly different from that measured in oocytes expressing Ca$_V$2.3 alone (*t* test; $P < .01$) (see Table S2 for details).

Consequently, we co-injected these proteins together with the cRNA-encoding Ca$_V$2.3 subunit (co-injection) and indeed found that inactivation was accelerated (Fig. 7 *A* and *B*) and the steady-state inactivation curve shifted toward more negative potentials (Fig. 7 *C* and *D* and Table S2). These findings indicate that the recombinant proteins are properly folded, and that after posttranslational modifications during biogenesis of the channel complex, Ca$_V\beta$ can switch the phenotype conferred to Ca$_V$2.3 from slow-inactivating to fast-inactivating.

Discussion

We have demonstrated that the GK module of the VGCC β subunit recapitulates key modulatory properties of the full-length protein, and thus Ca$_V\beta$-GK emerges as a functional competent domain. This implies that Ca$_V\alpha_1$–GK interaction suffices for channel gating regulation. Moreover, we have shown that regulation by GK is abolished by a mutation of the AID sequence, consistent with the idea that the AID–GK binding surface is critical for channel modulation (26). Although our size-exclusion chromatography and sucrose gradient analysis revealed that purified GK domains formed dimers in solution, the finding that Ca$_V\beta_{2a}$-GK covalently linked to a Ca$_V$1.2 pore-forming subunit fully recapitulated the activation properties of the channel (Fig. 3) proves that the functional unit is a single GK molecule. Our experiments also demonstrate that Ca$_V\beta$-GK can sustain the inhibition of voltage-dependent inactivation of Ca$_V$2.3 channels. The prevailing view is that this phenotype is conferred uniquely by Ca$_V\beta_{2a}$, because it is anchored to the membrane and constrains the movement of the inactivating particle encoded by loop I-II (15, 27). Our findings show that instead, inhibition of inactivation is not a unique feature of Ca$_V\beta_{2a}$, but rather is an inherent property of the GK module that appears to act as a brake to impair voltage-dependent inactivation. A corollary of this conclusion is that facilitation of inactivation by full-length Ca$_V\beta$ requires additional structural determinants to antagonize GK's brake-like effect. Full-length proteins, Ca$_V\beta_{1b}$ and Ca$_V\beta_{2a}$ C3,4S, were able to counteract the action of GK only when they were co-injected with the Ca$_V$2.3-encoding cRNA, as if these

PHYSIOLOGY

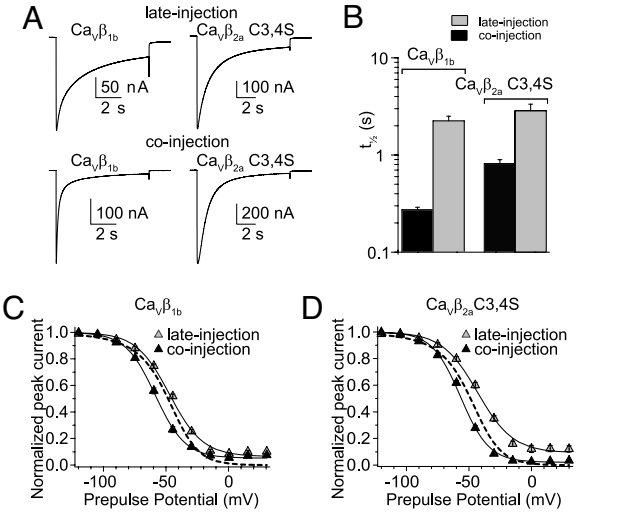

Fig. 7. The $Ca_V2.3$-inactivation phenotype induced by full-length $Ca_V\beta_{1b}$ and $Ca_V\beta_{2a}$C3,4S depends on the time of injection. (*A*) Representative current traces from oocytes expressing $Ca_V2.3$ channels with $Ca_V\beta_{1b}$ or $Ca_V\beta_{2a}$C3,4S injected either 2–7 h before recording (late injection) or co-injected with $Ca_V2.3$-encoding cRNA (co-injection). Currents were evoked by a 10-s pulse to 0 mV from a holding potential of −90 mV. (*B*) Average t½ for both of the subunit combinations shown in (*A*). Using $Ca_V\beta_{1b}$, the t½ values for co-injection (0.29 ± 0.02 s; $n = 11$) and late injection (2.19 ± 0.25 s; $n = 14$) differed significantly. This was true for experiments with $Ca_V\beta_{2a}$C3,4S as well (co-injection: 0.82 ± 0.08 s, $n = 13$; late injection: 2.86 ± 0.48 s, $n = 16$; *t* test; $P < .01$). (*C*) Steady-state inactivation curves from oocytes either co-injected or late-injected with $Ca_V\beta_{1b}$. The continuous lines correspond to the Boltzmann distributions that best describe each set of data. For comparison, the Boltzmann distributions that best describe the $Ca_V2.3$ data from Fig. 5 are shown (dashed lines). (*D*) As in *C*, but for $Ca_V\beta_{2a}$C3,4S. With both proteins, the V½ values from the co-injection experiments were significantly more negative than those from the late-injection experiments (*t* test; $P < .01$). For $Ca_V\beta_{2a}$ C3,4S, the V½ values from both the late-injection and co-injection experiments were significantly different from those values for $Ca_V2.3$ alone (*t* test; $P < .01$). The V½ value for $Ca_V\beta_{1b}$ differed from that of $Ca_V2.3$ alone only in the co-injection experiments. With both proteins, t½ values in late-injection and co-injection experiments differed significantly from each other and from those values for $Ca_V2.3$ alone (*t* test; $P < .01$) (see Table S2 for details).

determinants were acquired within a restricted time window during channel biogenesis.

We envision that in cRNA or protein co-injection experiments, formation of the $Ca_V\alpha_1$-$Ca_V\beta$ complex in early compartments, such as the endoplasmic reticulum, allows the necessary chemical or structural modifications to counteract GK's brake-like effect. Within this framework, palmitoylation may sequester $Ca_V\beta_{2a}$ to other membranous compartments early in the course of biogenesis, hindering the formation of $Ca_V\alpha_1$-$Ca_V\beta$ complexes in the compartment, which is permissible for these structural modifications. Alternatively, $Ca_V\beta$ protein may gradually switch to a fast-inactivation–conferring phenotype over a period of several days independent of its location or association state. In any case, we conclude that fast inactivation relies on further posttranslational modifications of $Ca_V\beta$, although the precise molecular mechanism remains to be identified.

In clear contrast to the protein injection experiments, we observed no modulation when $Ca_V\beta$-SH3-GK or $Ca_V\beta$-GK were co-injected as cRNA. Most likely, different parts of $Ca_V\beta$ are important to either efficient translation or stability of the protein in the oocyte cytoplasm. Indeed, modulation of inactivation by $Ca_V\beta_{2a}$-GK, injected as protein, is rather transient compared with that of the full-length protein, indicating a reduced lifetime. This may explain why previous attempts by either co-expressing or co-injecting the protein more than 24 h before the recordings yielded seemingly contradictory results (7–11). Although the time course of $Ca_V\beta_{2a}$-GK effect on $Ca_V1.2$ activation could not be determined, linking GK to $Ca_V1.2$ proved to be an effective strategy for stabilizing this module and increasing its potency. So far, we have been unable to express a concatamer of $Ca_V2.3$ with either the full-length $Ca_V\beta$ or the GK domain.

As new protein partners are discovered, the functional role of $Ca_V\beta$ is expanding rapidly (28, 29). We recently found that the SH3 module of $Ca_V\beta$ binds to the endocytotic protein dynamin (24), and now we report that the GK module regulates calcium channel function. Together, these findings introduce a new perspective on $Ca_V\beta$. Calcium entry through VGCCs on membrane depolarization ensures a transient change in intracellular calcium concentration that regulates diverse cellular functions. Integration of these different cellular processes must be tightly coordinated in living cells, and the domain architecture of $Ca_V\beta$, with its two functionally independent modules, appears particularly well suited for orchestrating calcium signaling. We suggest that whereas GK regulates calcium entrance, the SH3 domain links channel activity to other cellular processes by binding to additional proteins.

Materials and Methods

Construction of cDNA and Protein Expression. cDNA encoding the GK domain (residues 201–422), the SH3-GK core (residues 24–422) of rat β_{2a} (Swiss-Prot Q8VGC3–2), and the GK domain (residues 209–413) of the rat β_{1b} (Swiss-Prot P54283) were subcloned by polymerase chain reaction methods into a pRSET vector (Invitrogen). The predicted molecular masses of the $Ca_V\beta_{1b}$-GK, $Ca_V\beta_{2a}$-GK, and $Ca_V\beta_{2a}$-SH3-GK constructs, including the N-terminal His Tag, a transcript-stabilizing sequence, and the enterokinase cleavage recognition site, were 26.9 kDa, 28.6 kDa, and 48.2 kDa, respectively. $Ca_V\beta_{2a}$-SH3 was prepared as described previously (24). Full-length $Ca_V\beta_{2a}$, the mutant bearing two substitutions at positions 3 and 4 ($Ca_V\beta_{2a}$ C3,4S) and $Ca_V\beta_{2a}$-SH3-GK also were prepared as described previously (22). $Ca_V\beta_{1b}$, $Ca_V\beta_{1b}$-GK, and $Ca_V\beta_{2a}$-GK were expressed in bacteria and recovered from inclusion bodies as reported previously (30). The GK domains were refolded by batch dilution (11-fold dilution) in refolding buffer (400 mM L-arginine, 2 mM NaEDTA, 0.5 mM glutathione oxidized, and 100 mM Tris base [pH 7.0]) and subsequently purified by size-exclusion chromatography onto a Superdex S-200 column (GE Healthcare) preequilibrated with nondenaturing buffer (20 mM Tris, 300 mM NaCl, and 1 mM EDTA [pH 8.0]). Proteins were concentrated up to 0.1 mg/ml by ultrafiltration (Amicon Ultra-4 10 kDa MWCO), rapidly frozen, and stored at −80°C until use. The identity of the purified proteins was confirmed by mass spectrometry analysis performed in the mass spectrometry laboratory of the Department of Pharmacology and Toxicology, Medizinische Hochschule Hannover. The protein was digested by trypsin, and the peptides were analyzed with an Ultraflex MALDI-TOF/TOF mass spectrometer (Bruker Daltonics).

The loop I-II of $Ca_V1.2$ (Swiss-Prot P15381) fused to GST (GST–loop I-II) was prepared as described previously (30). YFP was fused to $Ca_V\beta_{2a}$-GK at its N terminus (YFP-$Ca_V\beta_{2a}$-GK) and subcloned into the pcDNA 3.1 vector. The cDNA encoding $Ca_V1.2$ was fused to the GK domain at the carboxyl-terminal end ($Ca_V1.2$- $Ca_V\beta_{2a}$-GK) by overlapping extension polymerase chain reaction, which incorporated the sequence ''MGRDLYDDDDKD'' at residue 2164 of $Ca_V1.2$. All constructs were verified by DNA sequencing.

Binding Assay. First, tsA201 cells were transfected with a YFP-$Ca_V\beta_{2a}$-GK or YFP-alone encoding vector and lysed after 24–36 h. Precleared cell extracts were incubated for 1 h with glutathione beads coupled to either GST–loop I-II or GST alone. The beads were pelleted and washed, and bound proteins were eluted with SDS/PAGE loading buffer. Proteins were then resolved on SDS/PAGE and visualized by fluorescence scanning (Typhoon imager; GE Healthcare).

Oocyte Injection and Electrophysiologic Recordings. cRNA was synthesized and *Xenopus laevis* oocytes were prepared, injected, and maintained as reported previously (30). The $Ca_V2.3$ encoding cDNA was sequenced; compared with the Swiss-Prot entry Q15878, the following changes were noted: I649M, W837L, P838A, and insertion of a glycine residue at position 839. The $Ca_V1.2$-subunit used in this study bears 60 aa deletion at the amino terminal (31). Electrophysiologic recordings were performed with the cut-open oocyte technique 4–6 days after cRNA injection and 1–7 hours after protein injection, as described previously (22). For details see SI *Materials and Methods*.

ACKNOWLEDGMENTS. We thank Christoph Fahlke and David Naranjo for insightful discussions and Andreas Pich for the mass spectrometry data. This work was supported by grants from the Deutsche Forschung Gemeinschaft Grant FOR 450 (to P.H.), Anillo de Ciencia y Tecnologia Grant ACT-46 (to A.N.), and German-Chilean Scientific Cooperation Program Grant DFG-CONICYT 2008 to P.H. and A.N.

1. Catterall WA (2000) Structure and regulation of voltage-gated Ca^{2+} channels. *Annu Rev Cell Dev Biol* 16:521–555.
2. Pragnell M, *et al.* (1994) Calcium channel β-subunit binds to a conserved motif in the I-II cytoplasmic linker of the α_1-subunit. *Nature* 368:67–70.
3. Harry JB, Kobrinsky E, Abernethy DR, Soldatov NM (2004) New short splice variants of the human cardiac Cavbeta2 subunit: Redefining the major functional motifs implemented in modulation of the Cav1.2 channel. *J Biol Chem* 279:46367–46372.
4. Opatowsky Y, Chen CC, Campbell KP, Hirsch JA (2004) Structural analysis of the voltage-dependent calcium channel beta subunit functional core and its complex with the alpha 1 interaction domain. *Neuron* 42:387–399.
5. Chen YH, *et al.* (2004) Structural basis of the alpha1-beta subunit interaction of voltage-gated Ca^{2+} channels. *Nature* 429:675–680.
6. Van Petegem F, Clark KA, Chatelain FC, Minor DL, Jr (2004) Structure of a complex between a voltage-gated calcium channel beta-subunit and an alpha-subunit domain. *Nature* 429:671–675.
7. Maltez JM, Nunziato DA, Kim J, Pitt GS (2005) Essential Ca(V)beta modulatory properties are AID-independent. *Nat Struct Mol Biol* 12:372–377.
8. Takahashi SX, Miriyala J, Colecraft HM (2004) Membrane-associated guanylate kinase–like properties of beta-subunits required for modulation of voltage-dependent Ca^{2+} channels. *Proc Natl Acad Sci USA* 101:7193–7198.
9. He LL, Zhang Y, Chen YH, Yamada Y, Yang J (2007) Functional modularity of the beta-subunit of voltage-gated Ca^{2+} channels. *Biophys J* 93:834–845.
10. McGee AW, *et al.* (2004) Calcium channel function regulated by the SH3-GK module in beta subunits. *Neuron* 42:89–99.
11. Richards MW, Leroy J, Pratt WS, Dolphin AC (2007) The HOOK-domain between the SH3- and the GK-domains of $Ca_V\beta$ subunits contains key determinants controlling calcium channel inactivation. *Channels* 1:92–101.
12. Olcese R, *et al.* (1994) The amino termini of calcium channel β subunits set rates of inactivation independently of their effect on activation. *Neuron* 13:1433–1438.
13. Qin N, *et al.* (1996) Identification of a second region of the beta-subunit involved in regulation of calcium channel inactivation. *Am J Physiol* 271:C1539–C1545.
14. Sokolov S, Weiss RG, Timin EN, Hering S (2000) Modulation of slow inactivation in class A Ca^{2+} channels by beta subunits. *J Physiol (Lond)* 527(Pt 3):445–454.
15. Restituito S, *et al.* (2000) The β2a subunit is a molecular groom for the Ca^{2+} channel inactivation gate. *J Neurosci* 20:9046–9052.
16. Hering S, *et al.* (2000) Molecular determinants of inactivation in voltage-gated Ca^{2+} channels. *J Physiol* 528(Pt 2):237–249.
17. Jones LP, Wei SK, Yue DT (1998) Mechanism of auxiliary subunit modulation of neuronal alpha1E calcium channels. *J Gen Physiol* 112:125–143.
18. Qin N, *et al.* (1998) Unique regulatory properties of the type 2a Ca^{2+} channel beta subunit caused by palmitoylation. *Proc Natl Acad Sci USA* 95:4690–4695.
19. Chien AJ, Carr KM, Shirokov RE, Rios E, Hosey MM (1996) Identification of palmitoylation sites within the L-type calcium channel beta2a subunit and effects on channel function. *J Biol Chem* 271:26465–26468.
20. Hurley JH, Cahill AL, Currie KP, Fox AP (2000) The role of dynamic palmitoylation in Ca^{2+} channel inactivation. *Proc Natl Acad Sci USA* 97:9293–9298.
21. Neely A, Wei X, Olcese R, Birnbaumer L, Stefani E (1993) Potentiation by the β subunit of the ratio of the ionic current to the charge movement in the cardiac calcium channel. *Science* 262:575–578.
22. Hidalgo P, Gonzalez-Gutierrez G, Garcia-Olivares J, Neely A (2006) The alpha 1-beta subunit interaction that modulates calcium channel activity is reversible and requires a competent alpha-interaction domain. *J Biol Chem* 281:24104–24110.
23. Dalton S, Takahashi SX, Miriyala J, Colecraft HM (2005) A single $Ca_V\beta$ can reconstitute both trafficking and macroscopic conductance of voltage-dependent calcium channels. *J Physiol* 567:757–769.
24. Gonzalez-Gutierrez G, Miranda-Laferte E, Neely A, Hidalgo P (2007) The Src homology 3 domain of the beta-subunit of voltage-gated calcium channels promotes endocytosis via dynamin interaction. *J Biol Chem* 282:2156–2162.
25. Berrou L, Klein H, Bernatchez G, Parent L (2002) A specific tryptophan in the I-II linker is a key determinant of beta-subunit binding and modulation in Ca(V)2.3 calcium channels. *Biophys J* 83:1429–1442.
26. Van Petegem F, Duderstadt KE, Clark KA, Wang M, Minor DL, Jr (2008) Alanine-scanning mutagenesis defines a conserved energetic hotspot in the $Ca_V\alpha_1$ AID-CaVbeta interaction site that is critical for channel modulation. *Structure* 16:280–294.
27. Berrou L, Bernatchez G, Parent L (2001) Molecular determinants of inactivation within the I-II linker of alpha1E (CaV2.3) calcium channels. *Biophys J* 80:215–228.
28. Hidalgo P, Neely A (2007) Multiplicity of protein interactions and functions of the voltage-gated calcium channel beta-subunit. *Cell Calcium* 42:389–396.
29. Zou S, Jha S, Kim EY, Dryer SE (2008) The beta1 subunit of L-type voltage-gated Ca^{2+} channels independently binds to and inhibits the gating of large-conductance Ca^{2+}-activated K^+ channels. *Mol Pharmacol* 73:369–378.
30. Neely A, Garcia-Olivares J, Voswinkel S, Horstkott H, Hidalgo P (2004) Folding of active calcium channel beta(1b) subunit by size-exclusion chromatography and its role on channel function. *J Biol Chem* 279:21689–21694.
31. Wei X, *et al.* (1996) Increase in Ca^{2+} channel expression by deletions at the amino terminus of the cardiac alpha 1C subunit. *Receptors Channels* 4:205–215.